XBn AND XBp DETECTORS BASED ON TYPE II SUPERLATTICES

P.C. Klipstein[1], Y. Benny[1], Y. Cohen[1], N. Fraenkel[1], S. Gliksman, A. Glozman[1], N. Hadari[1], I. Hirsh[1], M. Katz[2, 3], O. Klin[1], L. Langof[1], I. Lukomsky[1], I. Marderfeld[1], M. Nitzani[1], D. Rakhmilevich[1], S. Shusterman [2, 3], I. Shafir[3], I. Shtrichman[1], N. Sicron[2, 3], N. Snapi[1], and N. Yaron[1].

[1]SemiConductor Devices, P.O. Box 2250, Haifa 31021, Israel
[2]The Israel Center for Advanced Photonics, Yavne 81800, Israel
[3]Solid State Physics Department, Applied Physics Division, Soreq NRC, Yavne 81800, Israel
(*Email*: philip_k@scd.co.il)

ABSTRACT

XB*n* and XB*p* barrier detectors offer diffusion limited dark currents and high operating temperatures. Type II superlattices (T2SLs) based on either InAs/GaSb or InAs/InAsSb are ideal for their fabrication for two important reasons. First, their band gaps can be matched to the mid-wave infrared (MWIR) or long-wave infrared (LWIR) transparency ranges of the atmosphere, and second, their mini-band edges can be designed to create a large barrier for majority carriers and a negligible barrier for minority carriers, two requirements necessary for successful device operation. The main challenges are a short lifetime for both types of minority carrier in InAs/GaSb T2SLs, and non-metallic hole conductivity in both types of T2SL leading to a very low hole mobility. In this work we demonstrate how these challenges can be met, by exploiting very high electron mobilities in InAs/GaSb T2SLs, and a long Auger limited hole-lifetime in the gallium free T2SL for doping levels below 10^{15} cm^{-3}. Full MWIR focal plane array (FPA) operating temperatures are presented close to 130K, and robust LWIR FPA operation is demonstrated at 77K.

Key words: XBn, XBp, barrier detector, Type II superlattice, background limited performance, infrared, MWIR, LWIR.

INTRODUCTION

Type II superlattices (T2SL) are widely regarded as a realistic III-V alternative to mercury cadmium telluride for the fabrication of infrared detectors. Not only do they have a comparable absorption coefficient, but their band gap can be tuned through the short, mid, and long-wave infrared (S, M, LWIR) spectral ranges, by a suitable choice of layer thicknesses.[1] They can also be grown with a barrier architecture which excludes the depletion region from the narrow band gap photon absorbing active layer (AL), thereby suppressing the generation-recombination (GR) dark currents that usually limit the performance of conventional III-V photodiodes.[2,3,4,5] In this article, we present a short survey of the contrasting characteristics of barrier devices with *n*- and *p*-type active layer (AL) doping, based on two types of T2SL: InAs/GaSb and InAs/InAsSb. For *n*-type (*p*-type) AL doping, the device is known an XB*n* (XB*p*) detector, where the third letter stands for the doping of both the BL and AL, "B" stands for the majority carrier barrier, and "X" for the contact layer (CL) which can usually be made from more than one type of material and doping, so is given a "blank" letter.[5] In order to design T2SL barrier devices with the correct band alignments, we have developed a **k · p** simulation model with a number of novel features adapted for the III-V narrow band gap materials that are used in the superlattices.[6] It is used in conjunction with an optical transfer matrix and diffusion model to simulate the expected performance of the devices.[1] Together, these models allow the dark current and quantum efficiency of the barrier detector to be predicted from a basic knowledge of the T2SL period, stack thickness, diffusion length and minority carrier lifetime. Alternatively, from measurements of the dark current and quantum efficiency, the diffusion length and minority carrier lifetime can be estimated from fitting the model to the data. This procedure has been described previously, [7] and is used in the present work to probe the different conduction mechanisms in the T2SL devices that are studied.

InAs/GaSb T2SL XBp DETECTOR

At SCD we have developed high operability, 15μm pitch XB*p* barrier detector arrays based on *p*-type InAs/GaSb T2SLs, which led to the launch of our 640×512 format Pelican-D LW detector in 2017. With a cut-off wavelength of 9.3μm, this detector operates at 77K with a quantum efficiency (QE) above 50%, and a Noise Equivalent Temperature Difference (NETD) below 15 mK at F/2.7 and a 30 Hz frame rate.[8] In *p*-type T2SLs, the minority electrons are very mobile, exhibiting "metallic" conductivity with a large diffusion length, typically between 5 – 10 μm at 77K, which does not degrade at lower temperatures.[7] Some examples of device behavior are shown in Figure 1.

Figure 1(a) shows the typical profile of the conduction and valence bands in an XB*p* device at operating bias. Two types of T2SL are used in this device: InAs/GaSb for the AL, and InAs/AlSb for the barrier layer (BL). As mentioned in the Introduction, the BL has the same doping type as the AL, to avoid depletion of the narrow bandgap photon-absorbing layer and ensure that the current is diffusion limited.[5] At small biases, this doping configuration leads to a hole accumulation layer at the interface between the AL and the BL and an electrostatic barrier (EB) for minority electron transport from the AL to the CL. As the bias increases, the number of holes in the accumulation layer diminishes until the bands next to the BL become flat and the EB disappears. Just before the point at which the EB disappears is the typical operating bias of the device, allowing free passage of the diffusion limited dark current or the photon generated signal current to the CL. On further increasing the bias the AL begins to deplete and the dark current rises steeply due to the GR contribution from the depleted region.

Figure 1(b) shows the bias dependence of the dark current and QE at 77K for a back illuminated XB*p* test device without anti-reflection coating which had a cut-off wavelength of 9.8

μm and a contact area of 30x30 μm^2. Note that the QE is normalized to the mesa area and so is enhanced due to carrier diffusion from outside the mesa boundaries.[7] The dashed line shows the QE extrapolated to infinite device area. After an initial rise, the dark current becomes almost independent of voltage in the diffusion-limited regime close to an operating bias of 0.42V. At a bias of about 0.6V, the current starts to rise again, due to GR currents generated in the AL. The voltage independence of the QE at and above the operating bias in Figure 1(b) indicates that the diffusion length is larger than the AL thickness, which in this case is 4.5μm. The temperature dependence of the dark current, shown as an Arrhenius plot in Figure 1(c), demonstrates single slope diffusion behavior at 0.42V, changing to two-slope behavior at a higher bias of 1V, where the AL is partly depleted and the GR contribution dominates below 90K. The measured dark current points at 0.42V can be fitted to the Shockley formula, $J = en_i^2 L_0 / N_A \tau$ where L_0 is the thickness of the AL when this is less than the diffusion length, N_A is the AL doping, n_i is the intrinsic carrier concentration and τ is the minority carrier lifetime. N_A can be determined by measurements of the capacitance vs. voltage, and n_i can be calculated as a function of temperature from a **k** · **p** model as described in the Introduction.[7] This allows us to find the lifetime from the fit to the Shockley formula, yielding a value of τ = 7.5 ns. In spite of this short lifetime, the diffusion length in the growth direction, $L_{D\perp}$, is quite large. Its value at 77K is estimated by fitting the measured QE (extrapolated to infinite mesa dimension[7]) to its value simulated from **k** · **p** and optical transfer matrix models, yielding $L_{D\perp} \approx 6.6\mu m$. The electron mobility at 77K is then determined from the Einstein relation, $\mu = (e/kT\tau) L_{D\perp}^2 \approx 8800$ cm^2/Vs, which is a large value consistent with "metallic" conductivity. The large mobility is related to the very low electron effective mass in the T2SL, estimated from the **k** · **p** model to be $0.022m_0$, where m_0 is the free electron value.

An example of the imaging performance of the Pelican D LWIR focal plane array (FPA) detector is shown in Figure 2. The F/number used was 2.7 and the scene distance was 9.5 Km.

InAs/GaSb T2SL XBn DETECTOR

In contrast to the *p*-type devices, XB*n* barrier detectors based on *n*-type InAs/GaSb T2SLs exhibit much shorter diffusion lengths. An example of the band edge profile under operating conditions is shown in Figure 3(a). In Figure 3(b), the lack of a plateau in the plot of QE vs. bias at 110 K for MWIR devices with cut-off wavelengths close to 5.2 μm testifies to a very small diffusion length. From the data in this Figure, we use **k · p** and optical transfer matrix models as above, to estimate diffusion lengths of 0.65 and 0.8 μm, respectively, for devices with AL thicknesses of 1.5 and 2.6 μm. These diffusion lengths are very small because the minority holes are localized and conduct by hopping. At lower temperatures, where *kT* is much less than the localization energy, the diffusion length decreases towards zero.[9] The low diffusion length limits both the dark current and the QE. Therefore, although a fairly high background limited performance (BLIP) temperature can be reached of about 140K (when the dark current is equal to the photocurrent), the usefulness of such T2SL XB*n* devices is limited because the QE is then only about 25%. The localization can be explained by inhomogeneous energy fluctuations in the valence band which are greater than the hole mini-band width, according to the Mott Theory of the "metal-insulator transition".[10,11] Figure 3(c) shows single slope behavior for an Arrhenius plot of the operating dark current, from which a **k · p** fit[7] yields a minority carrier lifetime of 22ns. From this lifetime and a diffusion length of 0.8 μm, the hole mobility is estimated to be about 31 cm^2/Vs. This very low value is consistent with a hopping mechanism.[11]

InAs/InAsSb T2SL XBn DETECTOR

Similar or even lower values of the mobility are estimated for XB*n* devices based on gallium free InAs/InAsSb T2SLs. An example of the band profile at operating bias is shown in Figure 4 (a). However, in this case the hole lifetime can be up to two orders of magnitude longer than for InAs/GaSb T2SLs if the *n*-type doping is kept low. This is because the removal of GaSb eliminates GR centres which cause the lifetime to be very short.[12] The lifetime in the gallium free T2SL is Auger limited and can be as large as 10 μs for electron doping concentrations close to 10^{14} cm^{-3}.[13] Thus, even though their mobility is very small, this allows more time for the holes to reach the barrier layer where they can be collected. Therefore, in these XB*n* devices, the diffusion length and hence also the QE, can even be comparable with the values in the minority electron XB*p* devices described above.

The temperature dependence of the QE is shown in Figure 4(b) for two full MWIR XB*n* devices with AL doping levels of $n = 4\times10^{14}$ and 9×10^{15} cm^{-3}. The QE is much larger for the device with the lower doping because it has a longer lifetime, but in both cases it decreases rapidly with temperature due to the carrier localization. The lifetimes can be estimated as above by fitting the $\mathbf{k}\cdot\mathbf{p}$ model to the single slope Arrhenius plots of the dark current shown in Figure 4(c). Values of 10 μs and 200 ns are found, respectively, for the devices with low and high AL doping.

Based on the InAs/InAsSb T2SL XB*n* technology, we have fabricated a full MWIR InAs/InAsSb XBn FPA detector with a 15 μm pitch and a format of 640×512. Figure 5 shows a series of images registered at different temperatures with this detector in a test Dewar using F/3.2 optics. Excellent image quality can be observed up to the operating temperature of nearly 130K. The BLIP temperature is close to 140K and the QE is above 50%, which is comparable to that in our InAs/GaSb XB*p* detectors.

CONCLUSIONS

Both InAs/GaSb and InAs/InAsSb T2SLs can be used as the AL in barrier devices to produce high performance FPA detectors with a large QE operating in the MWIR or LWIR. Both kinds of T2SL exhibit absorption coefficients comparable with MCT although the gallium free T2SL has the weakest absorption of the three materials and usually requires a slightly thicker absorbing layer.[1]

An InAs/GaSb XB*p* architecture can be used for both MWIR and LWIR wavelength ranges. This design has a wide conduction mini-band with a low effective mass, ensuring that the minority electrons exhibit "metallic" conductivity. With a typical electron mobility of nearly 10,000 cm^2/Vs at 80K in an LWIR T2SL, large diffusion lengths of nearly 7 μm are observed, even though the lifetime of ~7.5 ns is very short. This device architecture is currently deployed in our production VGA format Pelican-D LWIR FPA detector, which operates at 77K with background limited performance.[14]

In the MWIR, higher XB*p* operating temperatures close to 120 K have been demonstrated from the dark current. A similar operating temperature has been observed with the XB*n* architecture, but the QE of the InAs/GaSb T2SL is then only about ~25% at 110K. The reason for this is a short lifetime of ~22 ns combined with a very low minority hole mobility of only ~30 cm^2/Vs, leading to submicron diffusion lengths. The low mobility is caused by the narrow valence mini-band which exhibits non-metallic conduction. The carriers are then localized and conduct by hopping, eventually freezing out as the temperature is lowered.

The same conduction mechanism exists for the holes in gallium free, InAs/InAsSb T2SL XB*n* detectors. However, here the lifetime is not GR limited as in the InAs/GaSb T2SL, but Auger limited which allows for much larger values when the doping is low. For doping of $4x10^{14}$ cm^{-3}, we

have estimated a lifetime of 10 μs which leads to hole diffusion lengths comparable with those of the electrons in the *p*-type InAs/GaSb T2SL.

In summary, barrier detectors based on both InAs/GaSb and InAs/InAsSb T2SLs perform with background limited sensitivity, both in the full MWIR wavelength range where they can exhibit stable operation according to strict production criteria at temperatures as high as 130K, and also in the LWIR wavelength range, where they offer robust performance at 77K.

ACKNOWLEDGEMENTS

The authors acknowledge technical support from Mr. I. Bogoslavski, Mr. Y. Caracenti, Mr. A. Franco, Mr. M. Grinberg, Mr. S. Greenberg, Mr. D. Gur, Ms. N. Hazan, Ms. L Krivolapov, Ms. M. Menahem, Ms. H. Moshe, Mr. Y. Osmo, Mr. E. Sandik, and Ms. H Schanzer, and who have all contributed to the successful growth, processing, packaging and characterization of the materials and devices.

Conflict of Interest:

The authors declare that they have no conflict of interest.

FIGURE CAPTIONS:

Figure 1

(a) Band profile at operating bias for a T2SL based *p*B*p* device in which the BL is intentionally doped with the same type as the AL (US patent 8,014, 012) (b) Dark current density and QE vs. bias for a back illuminated 30 × 30 μm^2 device with a cut-off wavelength of 9.8 μm at 77 K and no anti-reflection coating. Dashed line shows QE in the limit of infinite device area (black body illumination over wavelength range 7.6 – 9.8 μm) (c) temperature dependence of the dark current at the operating bias of 0.42V, and at a higher bias of 1.0V where the GR contribution becomes evident at low temperatures.

Figure 2

Image registered with a 15μm pitch, 640×512 Pelican-D LWIR FPA. The F/number was 2.7 and the scene distance was 9.5 Km.

Figure 3

(a) Band profile at operating bias of an *n*B*n* device with an InAs/GaSb T2SL AL, in which the BL is intentionally doped with the same type as the AL (US patent 8,014, 012) (b) Bias dependence of QE at 110 K in the wavelength range $3.2 \leq \lambda \leq 3.6$ μm, for *n*B*n* devices with no anti-reflection coating and a short period T2SL AL of thickness 1.5 μm (solid line) and 2.6 μm (broken line), respectively (c) temperature dependence at

operating bias of the diffusion limited dark current in the device with a 2.6 μm AL, and fit to a k · p model with a minority carrier lifetime of 22 ns.

Figure 4

(a) Band profile at operating bias of an *n*B*n* device with an InAs/InAsSb T2SL AL, in which the BL is intentionally doped with the same type as the AL (US patent 8,014, 012) (b) Quantum efficiency vs. temperature for two devices with an AL thickness of 3.5 μm and doping of 4×10^{14} cm^{-3} and 9×10^{15} cm^{-3} respectively. No anti-reflection coating was used and back illumination was performed with black body radiation over a wavelength range of 3.2 – 3.6 μm. (c) Temperature dependence at operating bias of the diffusion limited dark current for the devices with different AL doping levels, and fit to the Shockley diffusion current formula with a zero temperature bandgap wavelength of 5.61 μm, Varshni parameters of $\alpha = 3.5\times10^{-4}$ eV/K and $\beta = 280$ K, and the lifetimes listed in the legend.

Figure 5

Images registered at different temperatures with F/3.2 optics in a test Dewar for an InAs/InAsSb T2SL FPA with a 15 μm pitch and a format of 640 × 512.

FIGURE 1(a)

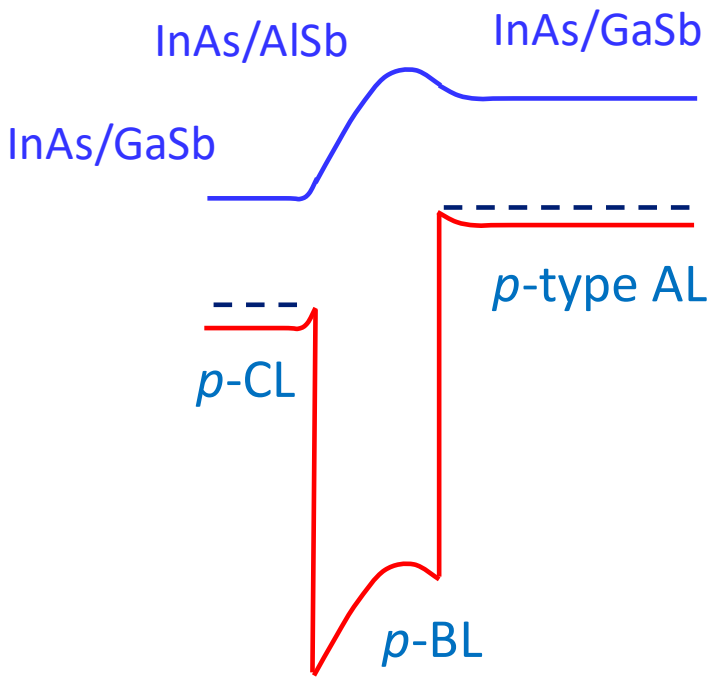

FIGURE 1(b)

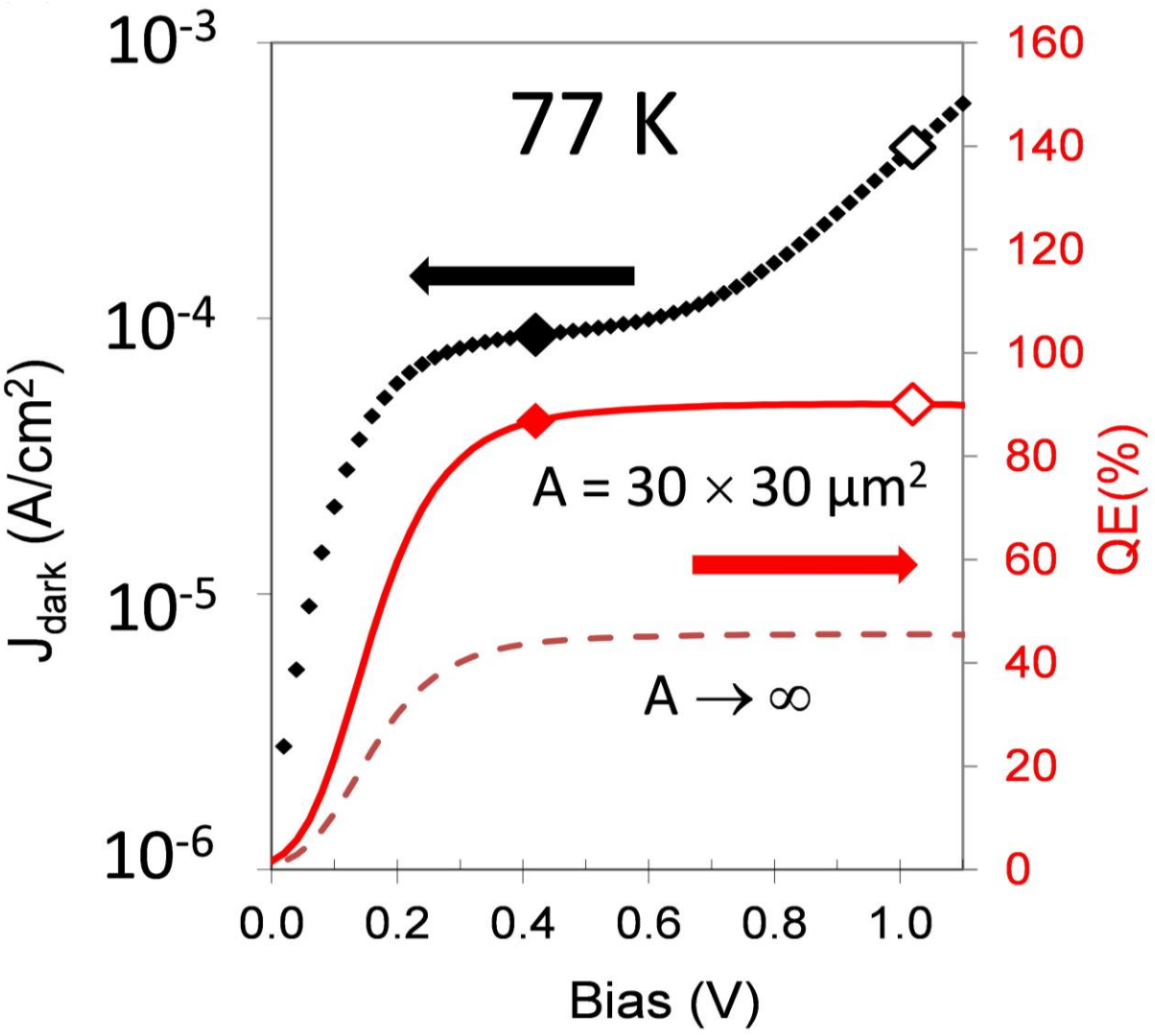
77 K
A = 30 × 30 μm²
A → ∞
J_dark (A/cm²)
QE(%)
Bias (V)
10⁻³
10⁻⁴
10⁻⁵
10⁻⁶
160
140
120
100
80
60
40
20
0
0.0
0.2
0.4
0.6
0.8
1.0

FIGURE 1(c)

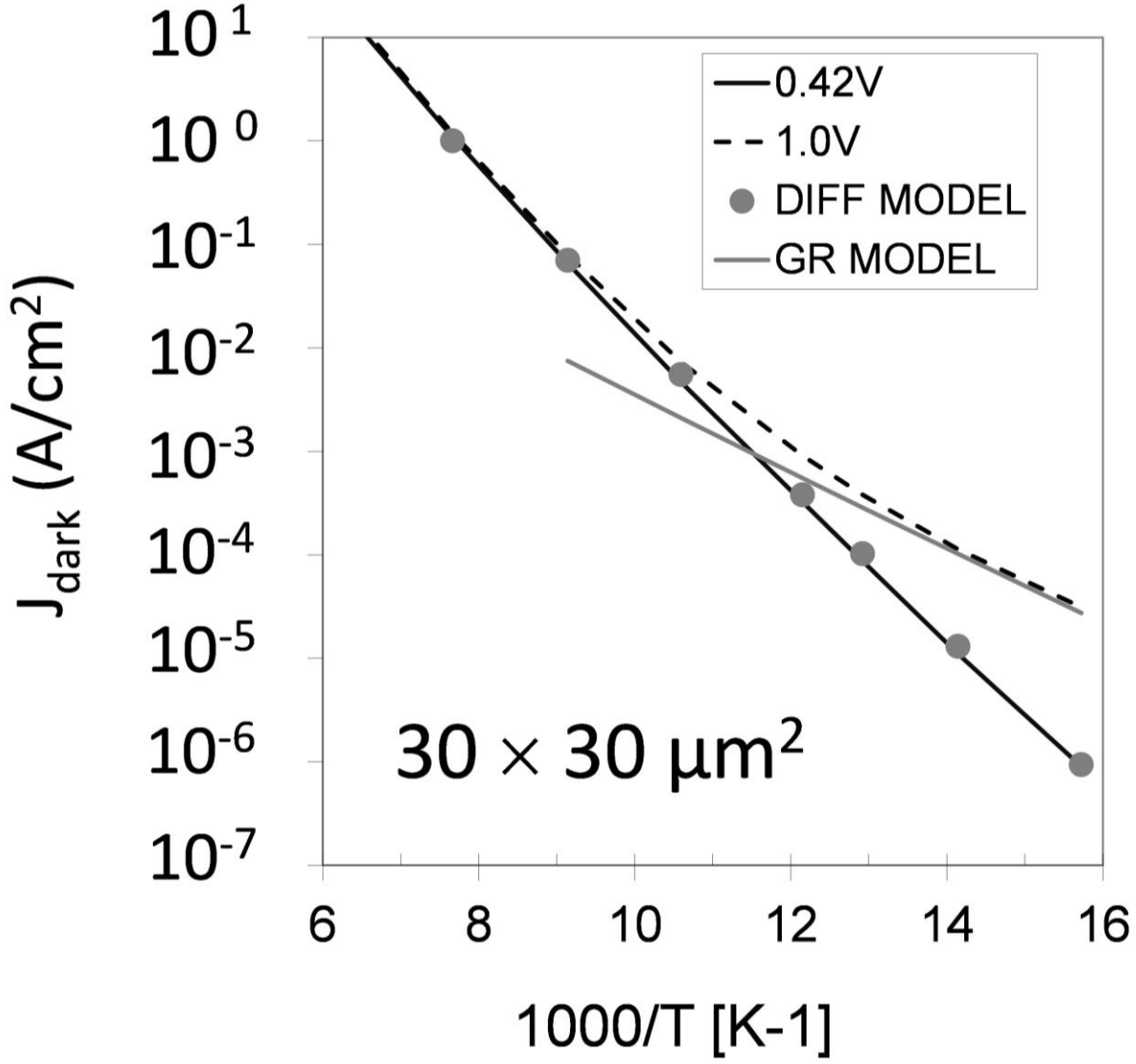
10^{1}
10^{0}
10^{-1}
10^{-2}
10^{-3}
10^{-4}
10^{-5}
10^{-6}
10^{-7}
J_{dark} (A/cm^2)
0.42V
1.0V
DIFF MODEL
GR MODEL
30 × 30 µm^2
6
8
10
12
14
16
1000/T [K-1]

FIGURE 2

FIGURE 3(a)

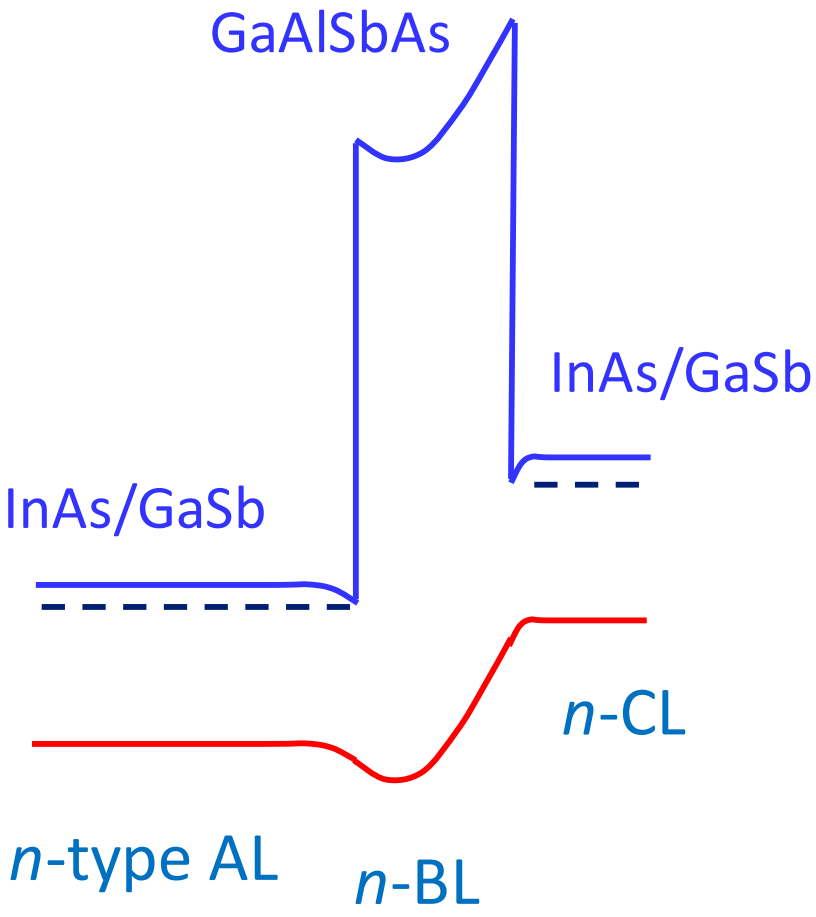

FIGURE 3(b)

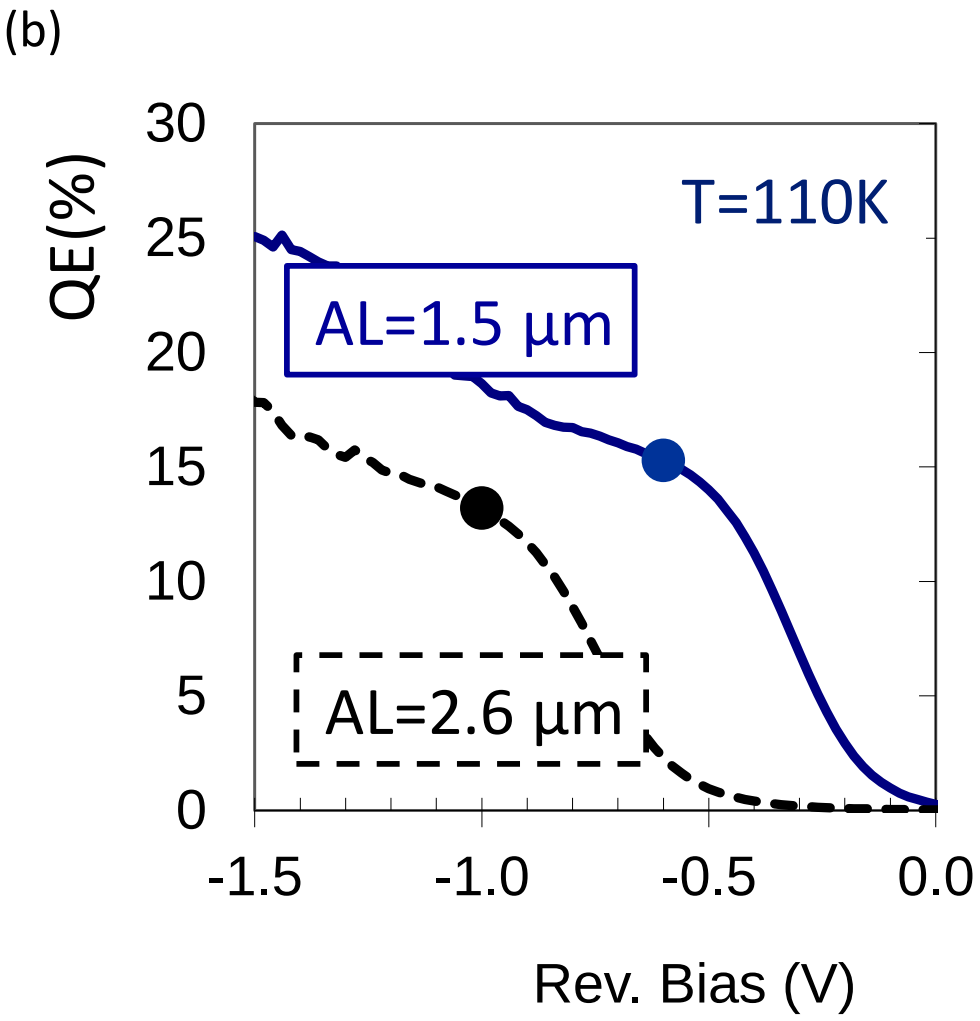

FIGURE 3(c)

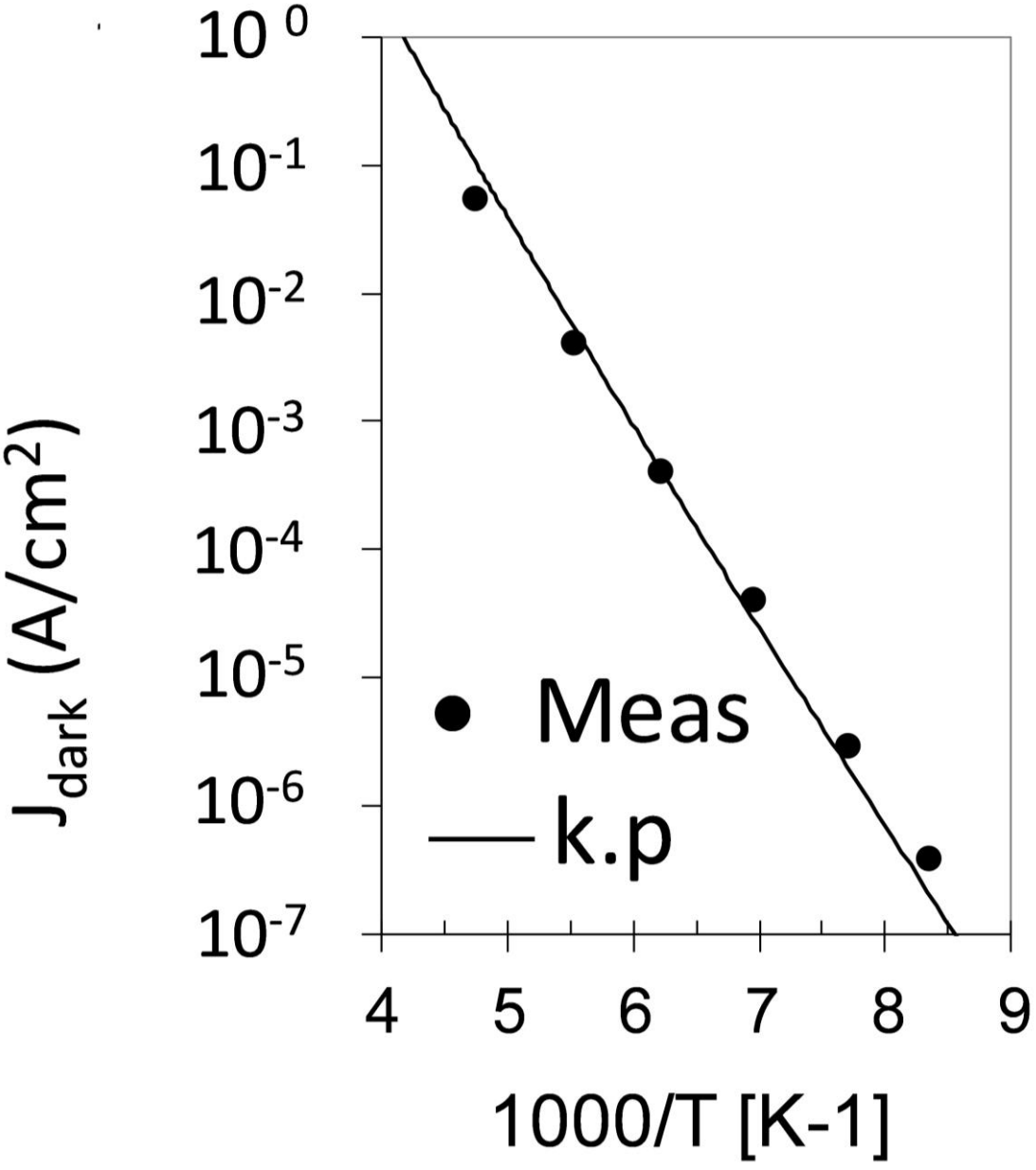
10^{0}
10^{-1}
10^{-2}
10^{-3}
10^{-4}
10^{-5}
10^{-6}
10^{-7}
J_{dark} (A/cm^2)
Meas
k.p
4
5
6
7
8
9
1000/T [K-1]

FIGURE 4(a)

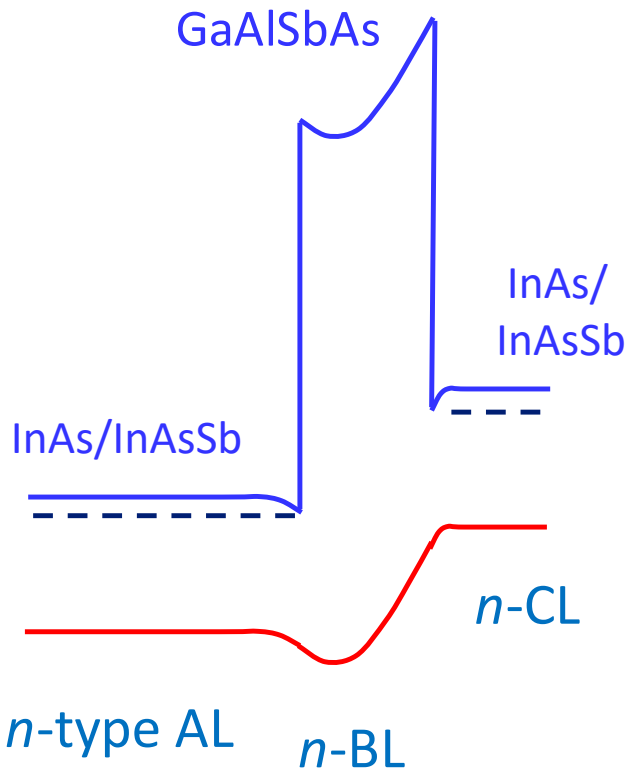

FIGURE 4(b)

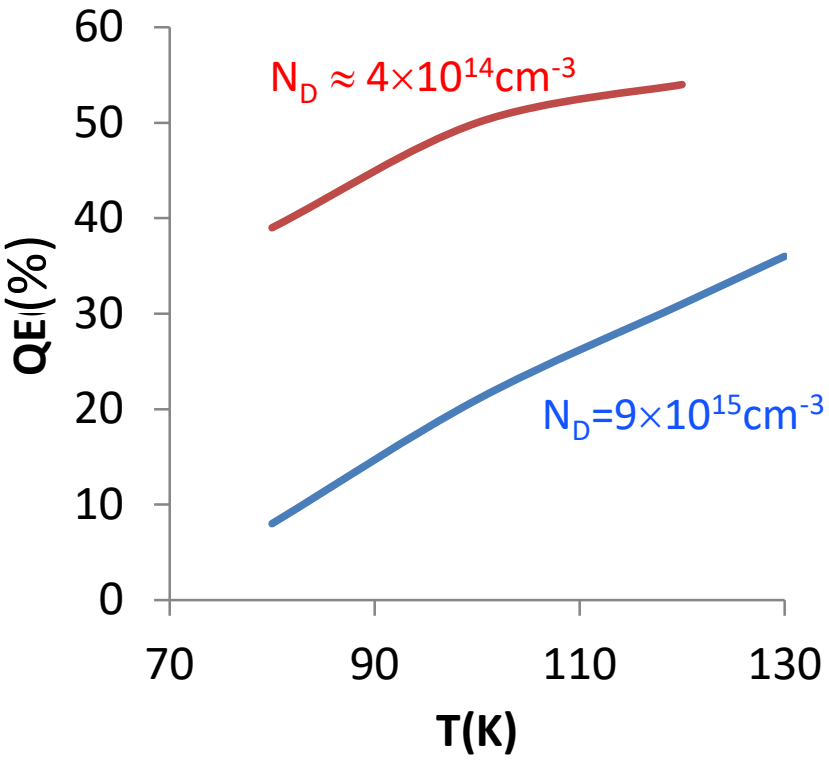

FIGURE 4(c)

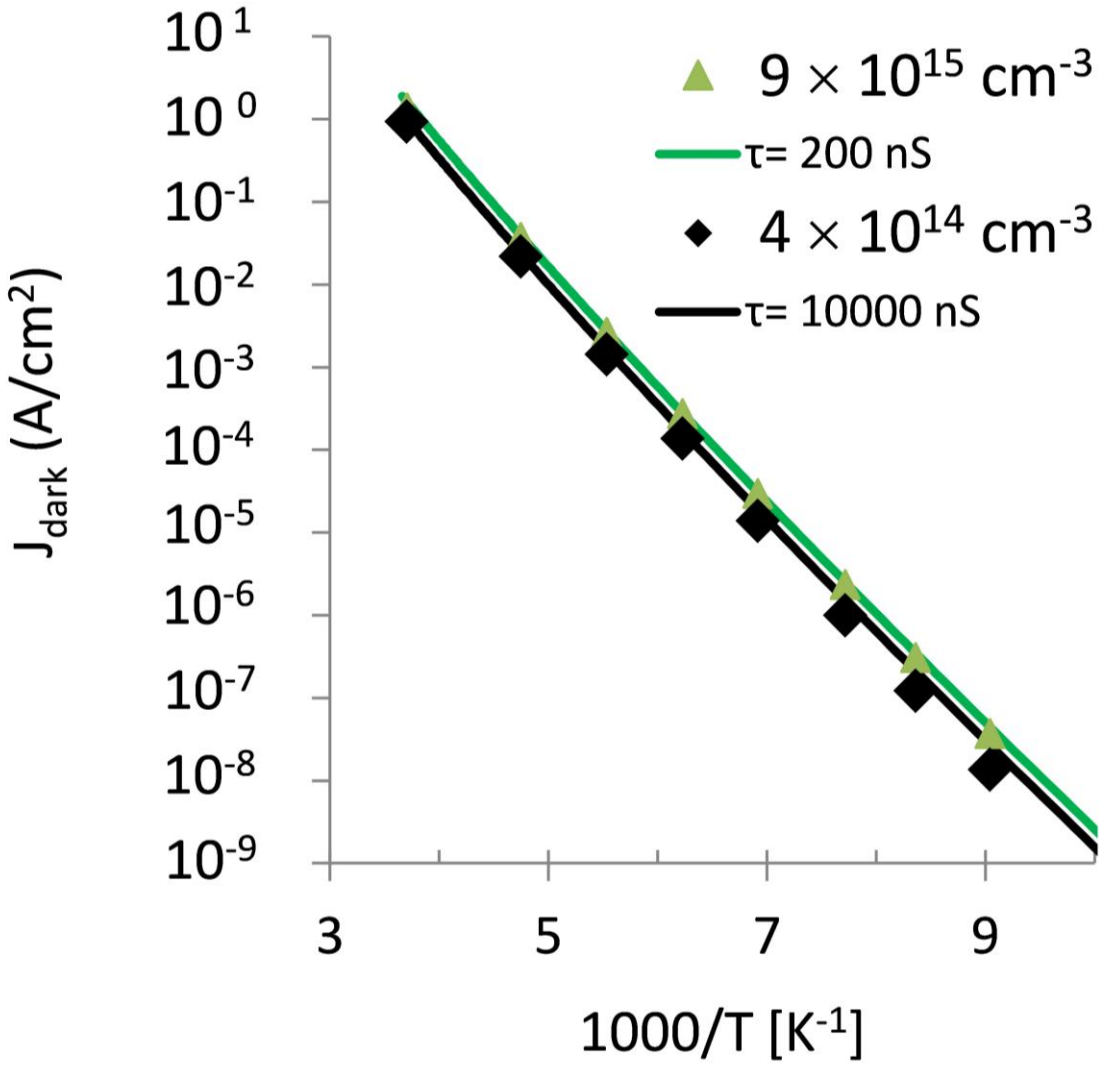
10^{1}
10^{0}
10^{-1}
10^{-2}
10^{-3}
10^{-4}
10^{-5}
10^{-6}
10^{-7}
10^{-8}
10^{-9}
J_{dark} (A/cm^2)
9×10^{15} cm^{-3}
τ= 200 nS
4×10^{14} cm^{-3}
τ= 10000 nS
3
5
7
9
1000/T [K^{-1}]

FIGURE 5

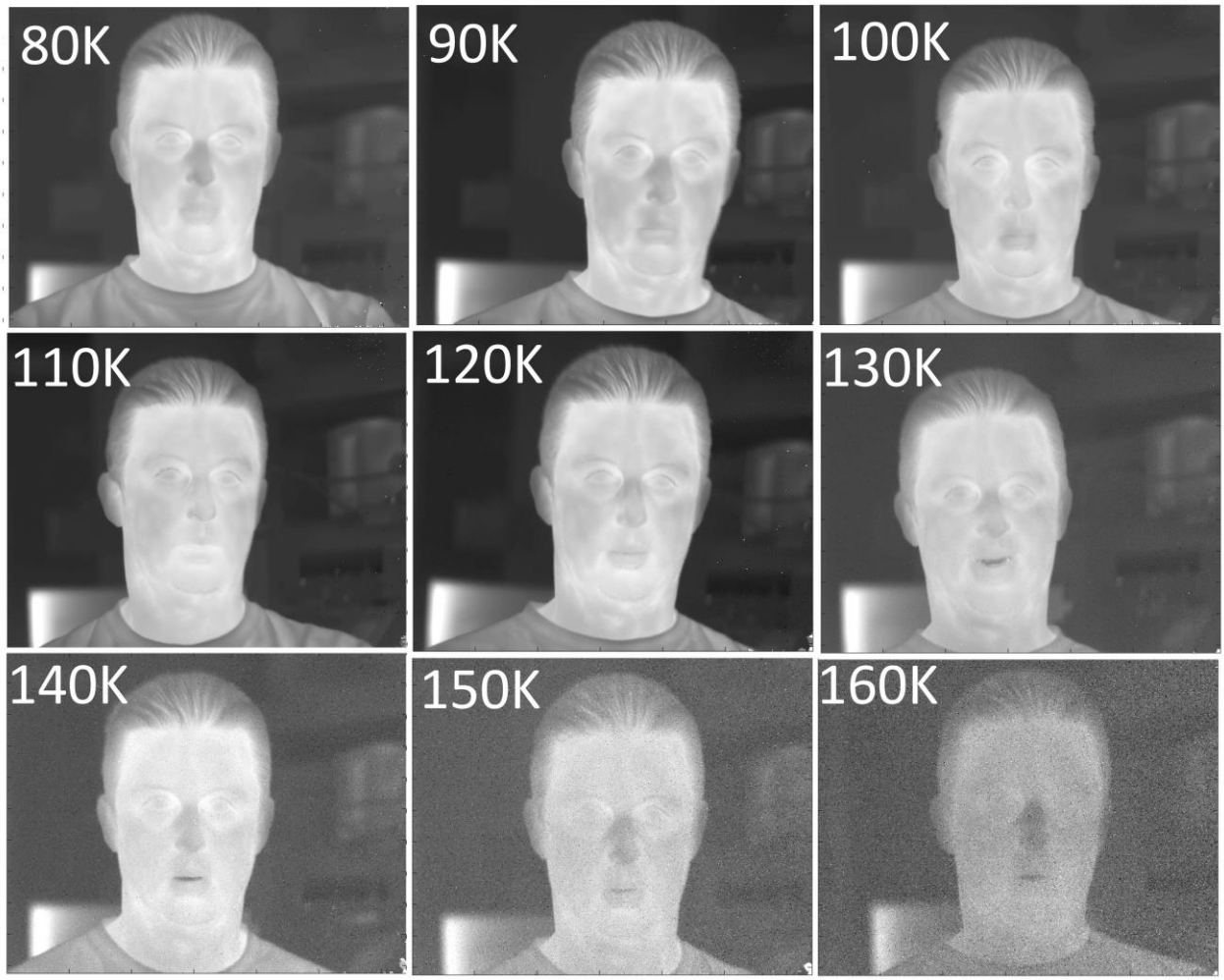

REFERENCES

1. PC Klipstein, Y Livneh, A Glozman, S Grossman, O Klin, N Snapi, E Weiss "*Modeling InAs/GaSb and InAs/InAsSb superlattice infrared detectors*", Journal of electronic materials **43**, 2984 (2014)
2. P.C. Klipstein "*Depletionless Photodiode with Suppressed Dark Current*…", US Patent 7,795,640 (2 July 2003)
3. P.C. Klipstein "*Unipolar semiconductor photodetector with Suppressed Dark Current…*", US Patent 8,004,012 (6 April 2006)
4. P.C. Klipstein, "*Semiconductor barrier photo-detector*" US Patent 9,627,563 (22 April 2013)
5. P.C. Klipstein *"XBn Barrier Photodetectors for High Sensitivity and High Operating Temperature Infrared Sensors*", Proc. SPIE **6940**, 6940-2U (2008)
6. Y. Livneh, P.C. Klipstein, O. Klin, N. Snapi, S. Grossman, A. Glozman and E. Weiss "*k· p model for the energy dispersions and absorption spectra of InAs/GaSb type-II superlattices*" Phys. Rev. B **86**, 235311 (2012); ibid, "*Erratum*" Phys. Rev. B **90**, 039903 (2014)
7. P.C. Klipstein, Y. Benny, S. Gliksman, A. Glozman, E. Hojman, O. Klin, L. Langof, I. Lukomsky, I. Marderfeld, M. Nitzani, N. Snapi, E. Weiss, "*Minority carrier lifetime and diffusion length in type II superlattice barrier devices*" Infrared Physics & Technology **96**, 155 (2019)
8. P.C. Klipstein, E. Avnon, D. Azulai, Y. Benny, R. Fraenkel, A. Glozman, E. Hojman, O. Klin, L. Krasovitsky, L. Langof, I. Lukomsky, M. Nitzani, I. Shtrichman, N. Rappaport, N. Snapi, E. Weiss, and A Tuito, "*Type II superlattice technology for LWIR detectors" Proc. SPIE* **9819**, 9819-0T (2016)
9. F. Bertazzi, A. Tibaldi, M. Goano, J. Alberto G. Montoya and E. Bellotti "*Nonequilibrium green's function modeling of type-II superlattice detectors and its connection to semiclassical approaches*" Phys. Rev. Applied **14**, 014083 (2020)
10. N.F. Mott "*Metal-Insulator transitions*", Chapter 1, section 1.7, pp. 30-40, 1st Edition, Taylor and Francis: London (1974)
11. P. C. Klipstein, Y. Benny, Y. Cohen, N. Fraenkel, R. Fraenkel, S. Gliksman, A. Glozman, I. Hirsch, O. Klin, L. Langof, I. Lukomsky, I. Marderfeld, B. Milgrom, H. Nahor, M. Nitzani, D. Rakhmilevich, L. Shkedy, N. Snapi, I. Shtrichman, E. Weiss, N. Yaron "*Type II superlattice detectors at SCD*" *Proc. SPIE* **11741**, 11741-0N (2021)
12. P.C. Klipstein, Y. Benny, Y. Cohen, N. Fraenkel, S. Gliksman, A. Glozman, I. Hirsh, L. Langof, I. Lukomsky, I. Marderfeld, B. Milgrom, M. Nitzani, D. Rakhmilevich, L. Shkedy, N. Snapi, I. Shtrichman, E. Weiss, N. Yaron "*Performance limits of III–V barrier detectors*" Journal of electronic materials **49**, 6893 (2020)
13. E. A. Kadlec, B. V. Olson, M. D. Goldflam, J. K. Kim, J. F. Klem, S. D. Hawkins, W. T. Coon, M. A. Cavaliere, A. Tauke-Pedretti, T. R. Fortune, C. T. Harris, and E. A. Shaner "*Effects of electron doping level on minority carrier lifetimes in n-type mid-wave infrared InAs/InAs$_{1-x}$Sb$_x$ type-II superlattices*", Appl. Phys. Lett. **109**, 261105 (2016)
14. P.C. Klipstein, E. Avnon, Y. Benny, E. Berkowicz, Y. Cohen, R. Dobromislin, R. Fraenkel, G. Gershon, A. Glozman, E. Hojman, E. Ilan, Y. Karni, O. Klin, Y. Kodriano, L. Krasovitsky, L. Langof, I. Lukomsky, I. Nevo, M. Nitzani,
I. Pivnik, N. Rappaport, O. Rosenberg, I. Shtrichman, L. Shkedy, N. Snapi, R. Talmor, R. Tessler, E. Weiss, and A. Tuito "*Development and production of array barrier detectors at SCD*", Journal of electronic materials **46**, 5386 (2017)